STUDY OF NEUTRAL ATOM TRAPS AND BOSE-HUBBARD MODEL

ANURAG KULSHRESTHA

A dissertation submitted for the partial fulfilment
of BS-MS dual degree in Science

Indian Institute of Science Education and Research Mohali
April 2014

Certificate of Examination

This is to certify that the dissertation titled **Study of Neutral Atom Traps and Bose-Hubbard Model** submitted by **Anurag Kulshrestha** (Reg. No. MS09022) for the partial fulfillment of BS-MS dual degree programme of the Institute, has been examined by the thesis committee duly appointed by the Institute. The committee finds the work done by the candidate satisfactory and recommends that the report be accepted.

Prof. Arvind | Prof. Jasjeet Bagla | Dr. Mandip Singh (Supervisor)

Dated: April 24, 2014

Declaration

The work presented in this dissertation has been carried out by me under the guidance of Dr. Mandip Singh at the Indian Institute of Science Education and Research Mohali.

This work has not been submitted in part or in full for a degree, a diploma, or a fellowship to any other university or institute. Whenever contributions of others are involved, every effort is made to indicate this clearly, with due acknowledgement of collaborative research and discussions. This thesis is a bonafide record of work done by me and all sources listed within have been detailed in the bibliography.

Anurag Kulshrestha

Dated: April 24, 2014

Acknowledgments

I would like to take this opportunity to thank Dr. Mandip Singh, my final year project supervisor, for guiding me throughout the year. I also acknowledge the sincere efforts put into this project by my friends Atul Mantri, Shivpal Kang, Vidit Agarwal, Harsh Katyayan and Mayank Mishra.

I want to thank my teachers at IISER-Mohali for teaching me the basics of Physics which have helped me in my understanding of the subject.

List of Figures

List of Tables

Contents

Abstract

In this work, I briefly describe the theory of magnetic trapping of neutral atoms and Bose-Hubbard model. In addition to that I append my calculations for different type of magnetic traps and their trapping potentials. This report is divided into 2 parts: the first half explains the magnetic trapping of neutral atoms, how a series of potential wells generated using three dimensional traps is useful to create a quantum register is described. The second half briefly describes the Bose-Hubbard model for a bosonic lattice. It explains two phases in a bosonic lattice which have contrasting properties, i.e. superfluid phase and Mott insulator phase. Furthermore, I calculate the wave functions and energies for a double well potential. The overlap of wave functions renders a finite tunneling probability from one site to the other.

Chapter 1

Magnetic Trapping of Neutral Atoms

The energy of interaction of a neutral atom in a magnetic field is very much weaker than the thermal energy of atoms at room temperature. Therefore, cooling of atoms is important to achieve trapping using magnetic field. It was in 1985 when magnetic trapping of neutral atoms was first achieved [1]. Since then this area of research has had both scientific and technological advancement resulting in the development of novel traps.

However, in order to understand the mechanism of trapping, it is essential to go over the spin properties which determine the interaction of atomic systems with external magnetic field.

1.1 Hyperfine Structure of Rubidium(87)

The energy level splittings in the **5S** orbital of ^{87}Rb are discussed in this section. The coupling between the the orbital angular momentum **L** of the outermost electron and its spin angular momentum **S** results in the fine structure. The total angular momentum is given by

$$\mathbf{J} = \mathbf{L} + \mathbf{S}. \tag{1.1}$$

The transitions $5^2P_{3/2} \rightarrow 5^2S_{1/2}$ and $5^2P_{1/2} \rightarrow 5^2S_{1/2}$ are fine-structure doublet components. Each of these two transitions have additional hyper-fine structure.
The hyper-fine structure is a result of coupling between the total angular momentum **J**

and the total nuclear angular momentum **I**. The total atomic angular momentum **F** is defined as

$$\mathbf{F} = \mathbf{J} + \mathbf{I}. \tag{1.2}$$

The magnitude of the total atomic angular momentum **F** can lie between

$$|J - I| \leq F \leq J + I \tag{1.3}$$

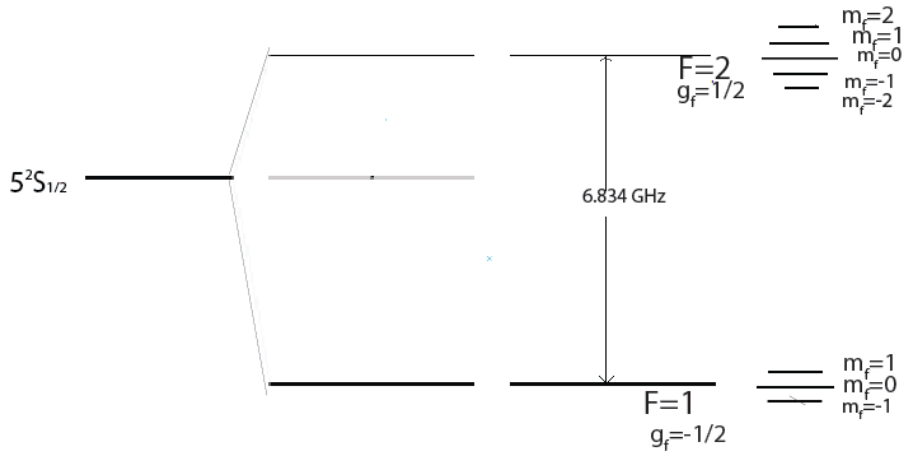

Figure 1.1: Hyper-fine structure for the state($5^2S_{1/2}$) of ^{87}Rb atom.

In case of first group neutral alkali atoms, the ground state of the outermost electron corresponds to $L = 0$. Consequently, $J = 1/2$ and F can either be $I + 1/2$ or $I - 1/2$. For $^{87}Rb, I = 3/2$, therefore we have $F = 1$ or $F = 2$. The situation might be different for other alkali atoms (eg. in the case of ^{85}Rb isotope, $I = 5/2$).
For the excited state in the D_2 line ($5^2P_{3/2}$), $F \in \{0, 1, 2, 3\}$ and in case of D_1 line, the excited state F is either 1 or 2.
In the absence of external magnetic field, the magnetic dipole interaction between nucleus and the electrons can remove the degeneracy between the two configurations $F = I \pm 1/2$. The interaction Hamiltonian can be represented as

$$H_{hf} = A\mathbf{I} \cdot \mathbf{J}, \tag{1.4}$$

where A is the coupling constant. The Hamiltonian H_{hf} can be expressed in terms of the quantum numbers I, J and F using the relation [12]

$$\mathbf{I} \cdot \mathbf{J} = \frac{1}{2}[F(F+1) - I(I+1) - J(J+1)], \tag{1.5}$$

where J=1/2 for the ground state of the alkali atoms. The splitting of the energy of the two hyperfine states $F = I \pm 1/2$ can now be calculated easily, and is given by

$$\Delta E = A\left(I + \frac{1}{2}\right). \tag{1.6}$$

However, in the presence of magnetic field, there is an extra magnetic interaction term added in the hamiltonian [12]:

$$H = A\mathbf{I} \cdot \mathbf{J} + 2\mu_B J_z B, \tag{1.7}$$

where $\mu_B = |e|\hbar/2m_e$ is the bohr magneton and application of magnetic field in done in the direction of z. F and m_F now become the good quantum numbers for the hamiltonian H. The interaction energy between the atom and the applied external magnetic field can be calculated using perturbation analysis [12]:

$$\langle F, m_F | 2\mu_B J_z B | F, m_F \rangle = g_L \mu_B m_F B, \tag{1.8}$$

where m_F is the eigenvalue of F_z or the magnetic quantum number and

$$g_L = \frac{F(F+1) + J(J+1) - I(I+1)}{2F(F+1)}, \tag{1.9}$$

is the Lande g factor [12].

1.2 Magnetic Interaction and Trapping

A particle with total angular momentum $\mathbf{F}$ and magnetic moment μ_B experiences a potential

$$V_{mag} = -\boldsymbol{\mu} \cdot \mathbf{B} = -g_F \mu_B m_F B \tag{1.10}$$

The magnetic moment precesses(Larmor precession $\omega_L = \mu_B B/\hbar$)about the magnetic field. Depending on the orientation of $\boldsymbol{\mu}$ relative to the direction of magnetic field $\mathbf{B}$, two cases can be distinguished:

- **Strong field seeking state:**

  If the magnetic moment and the magnetic field are aligned in the same direction, $V_{mag} < 0$. Therefore, V_{mag} decreases linearly with the magnitude of magnetic field. This is the reason why an atom trapped in a strong field seeking state is attracted towards the increasing fields.
  In this orientation the minima of the potential corresponds to the maxima of magnetic field. But, the Maxwell equations doesn't allow a finite divergence of magnetic field, and hence maxima of magnetic field in free space is forbidden.

- **Weak field seeking state:**

  On the contrary, if the magnetic moment and the magnetic field are aligned in opposite directions, $V_{mag} > 0$. Therefore the lower energies corresponds to lower magnetic fields. The atom is repelled from the regions with high magnetic field and attracted towards the lower fields. Hence, it is called a weak field seeking state. In this case the minima of the potential if found at the minima of the field. The fact that the minima of the modulus of magnetic field in free space is allowed by Earnshaw's theorem, trapping in this state can be done easily. This is the most common type of traps used to trap neutral atoms.

Majorana losses:
If the Larmor precession of the atom's magnetic moment about the external magnetic field is much faster than than the apparent change of magnetic field direction θ (in the rest frame of the moving atom), an adiabatic approximation can be applied.

$$\frac{d\theta}{dt} < \frac{\mu_B |\mathbf{B}|}{\hbar} \tag{1.11}$$

If the above condition is violated, which generally happens in regions of very small magnetic field, regions of trap loss are created due to *Majorana flips* or *spin flip transitions* into untrapped states.

1.3 Side guide

1.3.1 Quadrupole Trap:

Let us consider a system with a long thin wire parallel to the x-axis, passing through the origin($length = 1m$ and cross-sectional area = $0.25mm^2$) and carrying a current I = $2A$. In addition to that there is also a homogeneous bias field(B_b) applied in a direction perpendicular to the length of the wire [Figure 1.2]. The combination of this externally applied magnetic field and the circular field created by the wire, produces a 2 dimensional field minima in the form of a quadrupole field [Figure 1.3]. The bias field cancels the circular magnetic field of the wire along a line parallel to the wire at a distance

$$z_o = \frac{\mu_o I}{2\pi B_b}, \tag{1.12}$$

from the wire.

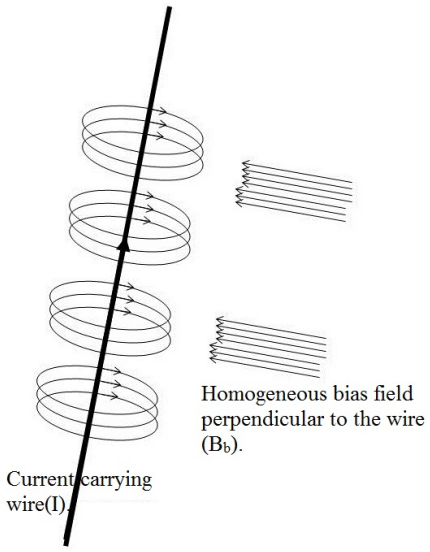

Figure 1.2: Application of homogeneous bias field perpendicular to the current carrying wire.

Atoms in the weak field seeking state can be trapped in this 2-dimensional quadrupole field and can be guided along the sides of the wire. The field gradient at the center of the trap is

$$\frac{dB}{dz}\,|_{z_o+\Delta z} \;= \frac{2\pi B_b^2}{\mu_o I}. \tag{1.13}$$

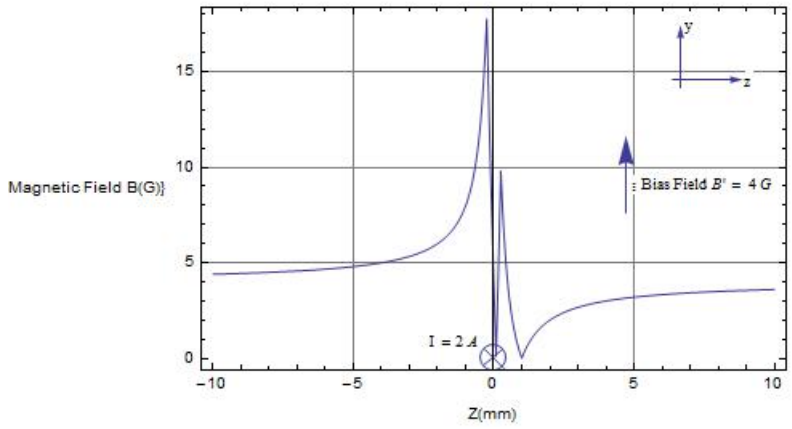

(a)

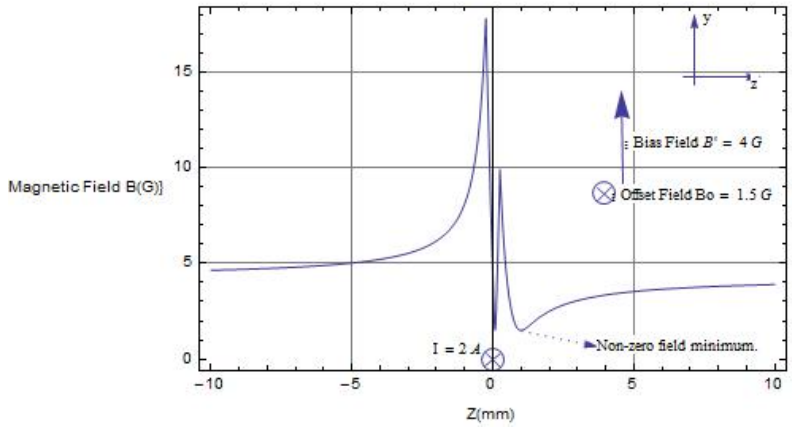

(b)

Figure 1.3: Magnetic field variation along Z-axis for quadrupole trap **(a)** and Ioffe-Prichard trap **(b)**.

1.3.2 Ioffe-Prichard Trap:

In the system described above, the field at the trap-center(the region of field minimum) is exactly zero. Consequently, there can be Majorana transitions between the trapped and the untrapped spin states.

To avoid these losses, a small magnetic field component, a field offset(B_{off}), can be added along the wire direction. Application of this field ensures that the degeneracy between the trapped and untrapped states is removed, as there is a non zero field minimum [Figure 1.3]. This potential is known as a Ioffe-Prichard trap [2] [3] [4].

Furthermore, the form of the potential at the minimum changes to harmonic. The curvature at the point of trap-minimum is [5]

$$\frac{d^2B}{br^2} = \frac{4\pi^2 B_b^2}{B_{off} I^2} = \frac{B_b^2}{z_o^2 B_{off}}, \tag{1.14}$$

and in the harmonic-oscillator approximation, the trap frequency is given by [5]

$$\frac{\omega}{2\pi} = \frac{1}{2\pi}\sqrt[2]{\frac{\mu_B g_F m_F}{M}\left(\frac{d^2B}{dr^2}\right)} \tag{1.15}$$

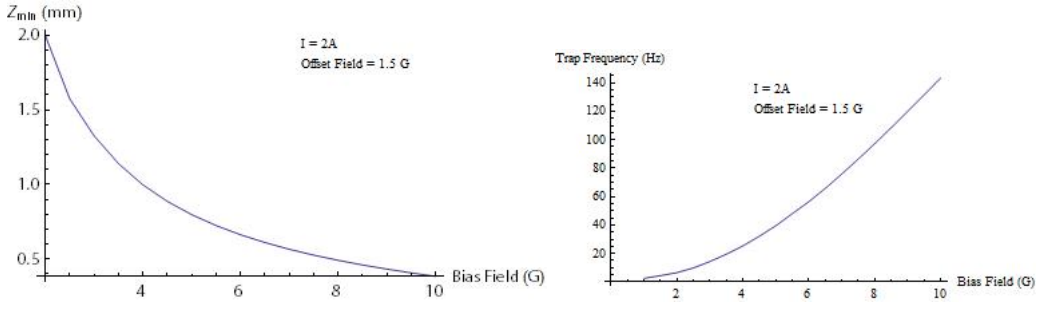

(a) **(b)**

Figure 1.4: Variation of z_o with bias-field(a), trap frequency with bias-field(b) at constant current and field offset in an I-P trap.

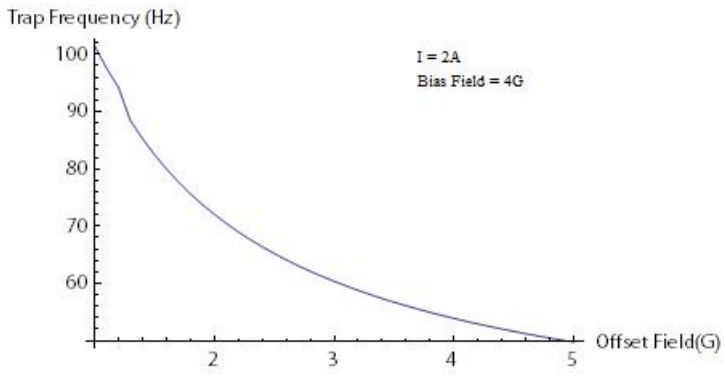

Figure 1.5: Variation of trap frequency with offset field at constant current and bias field in an I-P trap.

The variation of the trap frequency and z_o with bias-field and offset field can be be observed in the above figure. The dimensions of the wire, its orientation and the direction of application of bias and offset fields are the same as discussed in the section 1.3.1.

1.4 Bent Wire Traps

Three dimensional trapping can be achieved by extending the two dimensional trap discussed in section 1.3. To accomplish this, the current carrying wire is bent in the shape of either 'U' of 'Z' (as shown in the figure 1.6)[6][7][8]. If we apply a homogeneous magnetic field perpendicular to the central part of the wire(along positive-Y direction), it interacts with the circular magnetic field created due to the wire and results in the formation of a quadrupole trap same as before.

The x-component of the field produced due to the bent parts of the wire create endcaps for the wire guide and allows confinement along the its axis, while the y-component displaces the minimum of this field.

There can be an additional offset field applied in a direction parallel to the cross wire to adjust the field minimum (in case of the 'Z'-wire) or to vary the position of the trap center(in the case of a 'U'-wire). This is discussed in a more vivid manner in the following two subsections.

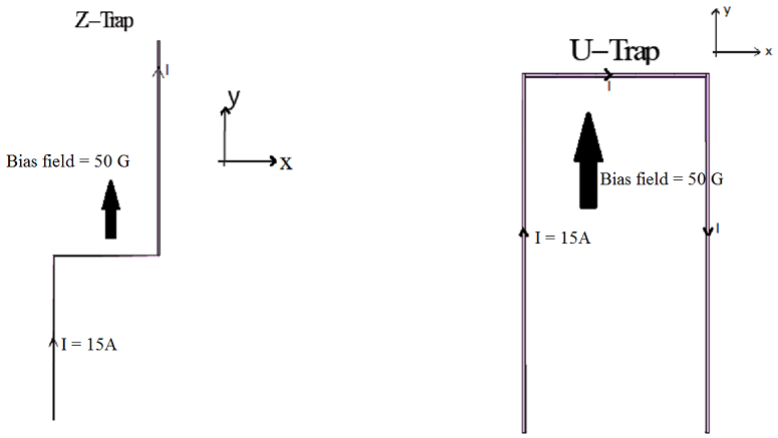

Figure 1.6: Wires bent in the shape of Z(left), and U(right) to form 3-dimensional traps. The length of the cross-wire in each case is 3mm and that of the each bent component is 6mm each.

1.4.1 U-Wire Trap

In case of the U-wire the contributions of the two bent parts cancel each other out at the trap center(figure 1.7), which form a 3-dimensional quadrupole trap at the zero field point i.e. trap center (figure 1.9).

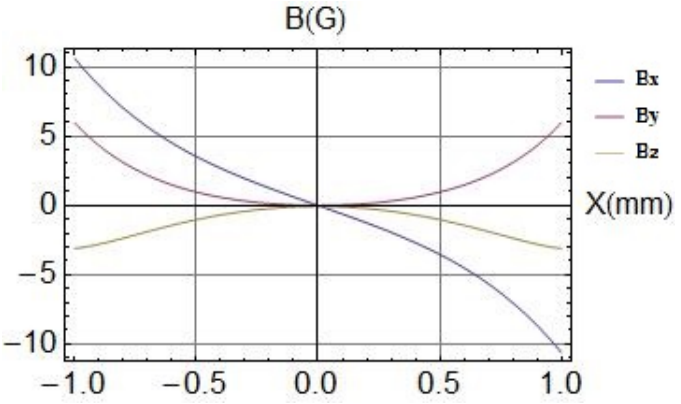

Figure 1.7: Variation of magnetic field components along the cross-wire(X) in a U-Trap. [Y=0, Z = trapcenter]

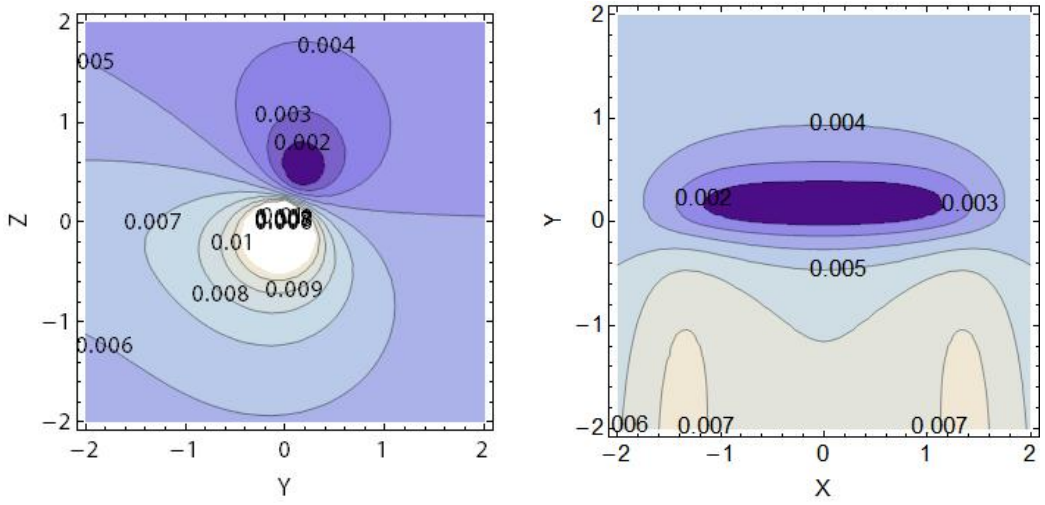

Figure 1.8: Contour plot showing a quadrupole trap formed at the trap center in a U-wire trap(left): the figure shows the variation of the magnetic field in the plane $X = 0$. The zero-point of the magnetic field occurs at $P_{tc} = (0, 0.1599mm, 0.5149mm)$. The variation of magnetic field in the plane parallel to the plane of the wire and passing through the trap center i.e. plane $Z = 0.5149mm$ (right). The current running along the wire is $I = 15A$, homogeneous bias field applied perpendicular to the cross-wire has a magnitude of $50G$.

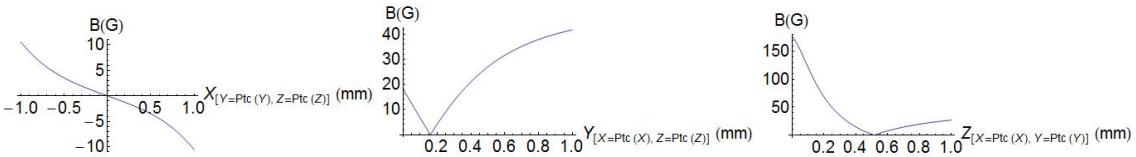

(a) **(b)** **(c)**

Figure 1.9: The magnetic field along the three mutually orthogonal lines passing through the trap center of the quadrupole trap: **B** along the line (Y=$P_{tc}(Y)$, Z= $P_{tc}(Z)$) **(a)**, **B** along the line (X=$P_{tc}(X)$, Z= $P_{tc}(Z)$) **(b)**, **B** along the line (X=$P_{tc}(X)$, Y= $P_{tc}(Y)$) **(c)**. The current running along the wire is $I = 15A$, homogeneous bias field applied perpendicular to the cross-wire has a magnitude of $50G$.

Effect of offset field and thickness of the wire on the U-trap

The external magnetic field can be rotated so as to apply a parallel component to the central part of the wire. There is still a quadrupole trap formed at the trap center same as before, the only difference being that the position of the trap center shifts in the direction of the applied magnetic field(figure 1.10).

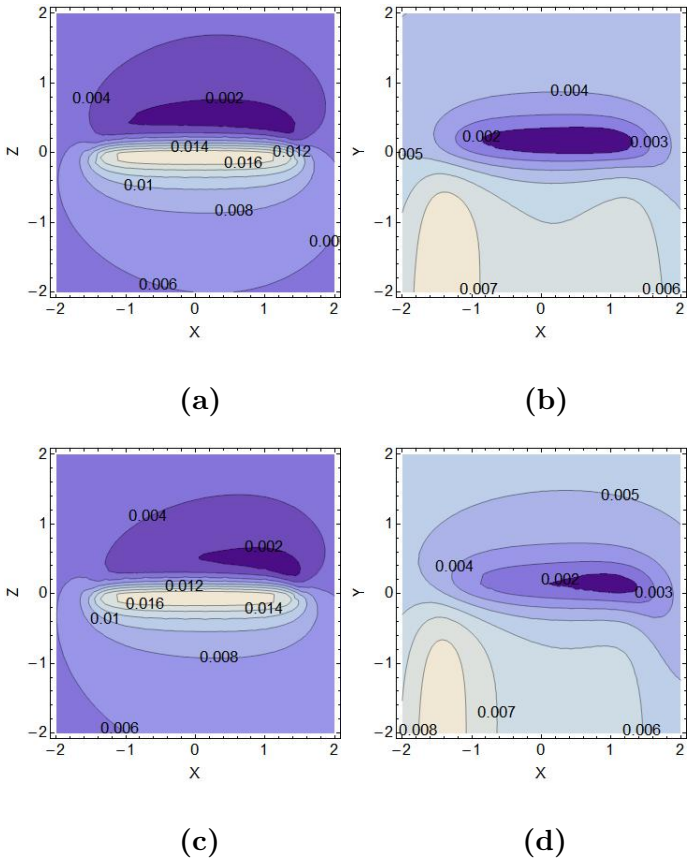

Figure 1.10: Shifting of the quadrupole trap center on rotation of applied external field. The rotation is done in such a manner that the magnetic bias field component perpendicular to the cross-wire remains the same in magnitude as before and an magnetic offset field component is introduced parallel to the cross-wire. The translation of the trap center can be observed in the X-Z plot at $Y = P_{tc_y}$) and X-Y plot at $Z = P_{tc_z}$: **(a),(b)** for offset field component=10G, and **(c),(d)** for offset field component=20G.

In order to construct the wire traps mentioned in the sections 1.3, 1.4.1 and in the ones to be discussed later, we have used a geometry similar to that of micro-fabricated wires. They have typically a rectangular cross section and an aspect ratio smaller than 1(width greater than height). We can see the effect of varying the width of the wire on the quadrupole trap in table 1.4.1 and figure 1.12.

Trap	Cross Wire	Current	Bias Field	Trap Center(P_{tc})	$B_y^{'}(P_{tc})$	$B_z^{'}(P_{tc})$	$B_x^{'}(P_{tc})$)
U_1	3mm	15A	50G	(0, 0.16mm, 0.515mm)	113.36 G/mm	98.24 G/mm	6.2 G/mm
U_2	8mm	15A	10G	(0, 3.46mm, 0.25mm)	7.78G/mm	13.9 G/mm	0.23 G/mm

Table 1.1: Magnetic field gradients for two different type of U-traps:$U_1 \rightarrow$ Uniform size of wires; and $U_2 \rightarrow$ cross-wire having relatively large width.

A magnetic trap is formed due to the interaction of magnetic fields. It's characteristics(such as the gradient at trap minimum for a quadrupole trap) are dependent upon 2 factors:

- the shape and size of the carrying current conductor(I); and
- the externally applied magnetic field($\mathbf{B}$).

In the following figure we see how the shape of the conducting wire changes the properties of the three dimensional quadrupole trap. If there is a U wire [figure1.11] having a much wider cross-wire as compared to the U-wire discussed above in figure 1.6, the shape of the trap changes which is manifested in their trap gradients (figure1.12.)
This however, is an approximate result as I have considered a constant flow of current in the wires which is not actually the case in reality. As we move up from the confluence of cross and side wire, the current decreases across the cross wire.

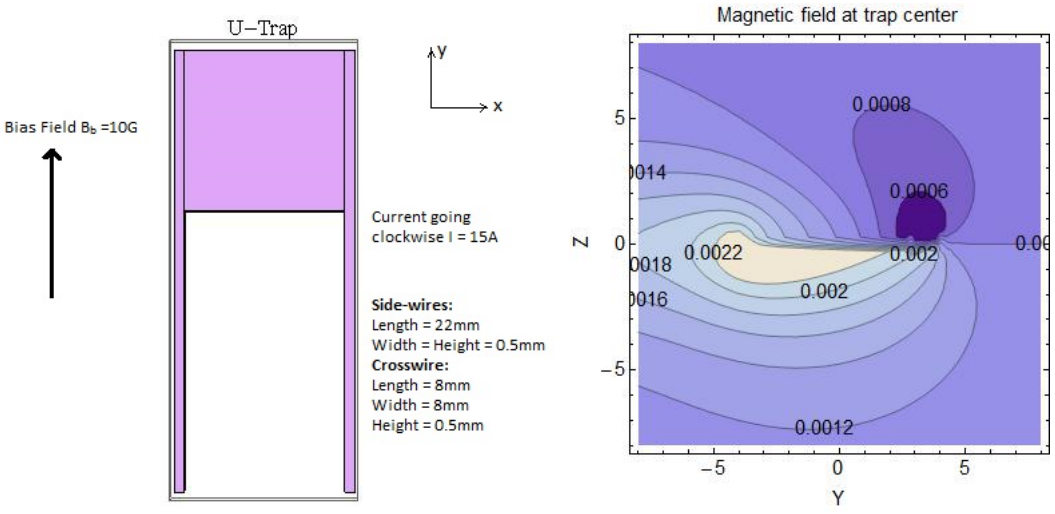

(a) **(b)**

Figure 1.11: U-wire with a cross wire having large width**(a)**. The zero-point of the magnetic field occurs at $P_{tc} = (0mm, 3.460mm, 0.252mm)$. The variation of magnetic field in the plane parallel to the plane of the wire and passing through the trap center i.e. plane $Z = 0.252mm$ **(b)**.

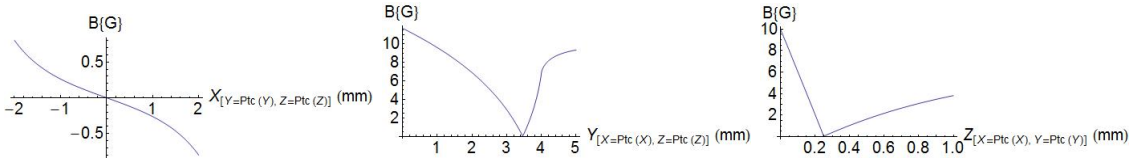

(a) **(b)** **(c)**

Figure 1.12: The magnetic field along the three mutually orthogonal lines passing through the trap center of the quadrupole trap: **B** along the line (Y=$P_{tc}(Y)$, Z= $P_{tc}(Z)$) **(a)**, **B** along the line (X=$P_{tc}(X)$, Z= $P_{tc}(Z)$) **(b)**, **B** along the line (X=$P_{tc}(X)$, Y= $P_{tc}(Y)$) **(c)**. The current running along the wire is $I = 15A$, homogeneous bias field applied perpendicular to the cross-wire has a magnitude of $10G$.

As a result of increasing the width of the cross-wire from 0.5mm to 8 mm, there is a significant decrease in the magnetic field gradients at the trap center of the quadrupole trap. The gradients for these two different U-trap are tabulated in the table 1.4.1. Therefore, we infer that the shapes and depths of the traps can be altered by changing the dimensions of the wires.

1.4.2 Z-Wire Trap

In the Z-wire scenario, the two contributions of the bent parts add up giving rise to a non-zero magnetic field at the trap center(figure 1.13). This new field contribution adds up quadratically with the the two dimensional quadrupole field, thereby resulting in an Ioffe-Prichard trap at the center.

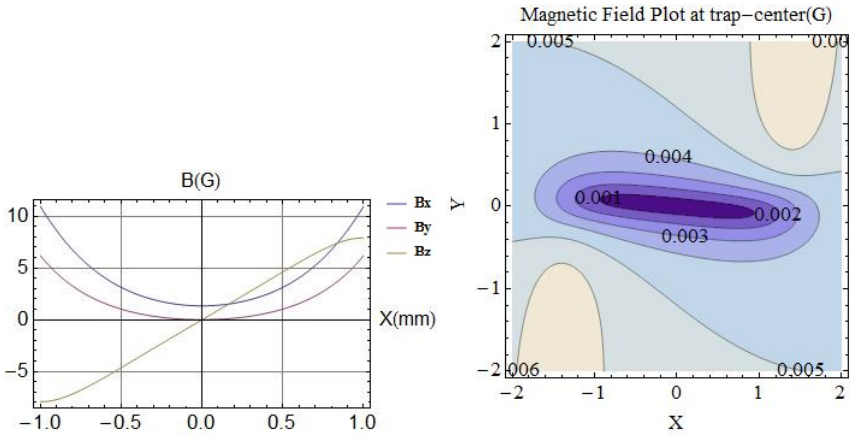

Figure 1.13: Variation of magnetic field components along the cross-wire in the plane Z = $P_{tc}(Z)$(left).B_x,B_y and B_z are components of magnetic field along X, Y and Z axis respectively. Contour-plot of magnetic potential due to the Z-wire trap creating 3-dimensional confinement(right). The variation of total magnetic field in the plane Z = $P_{tc}(Z)$. The current running along the wire is $I = 15A$, homogeneous bias field applied perpendicular to the cross-wire has a magnitude of $50G$. The additionally applied offset field has a magnitude of 5 G. The trap-center is located at $P_{tc} = (0mm, 0mm, 0.556mm)$

Unlike in the the case of a three-dimensional U-wire quadrupole trap, there is a non-zero trap minimum at the trap center in the of an Ioffe-Prichard trap created by a Z-wire trap. Therefore, in a Z-trap, a well defined curvature exists at the trap center.

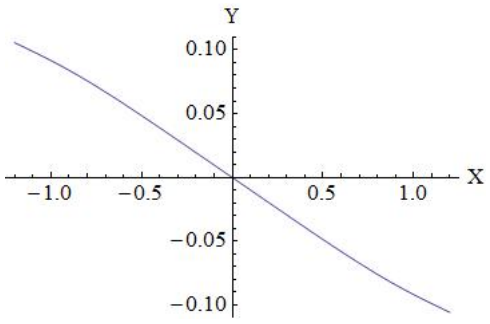

Figure 1.14: Line joining the field minima along the lines X = a; where $a \in [-1.2mm, 1.2mm]$

As I had already mentioned in section 1.4, an additional offset field in a direction parallel to the cross-wire is also applied in the Z-trap in order to shift the magnitude of magnetic field at the trap center(B_{tc}). Another way to say it would be that the externally applied magnetic field is rotated and adjusted to provide a component along the cross-wire.

In the three dimensional Z-trap, the line corresponds to axial direction and the line perpendicular to it corresponds to the radial direction.

The Z-trap provides confinement axially as well as radially. The plots for the magnetic field along the axial and radial directions are shown in the following figure(1.15).

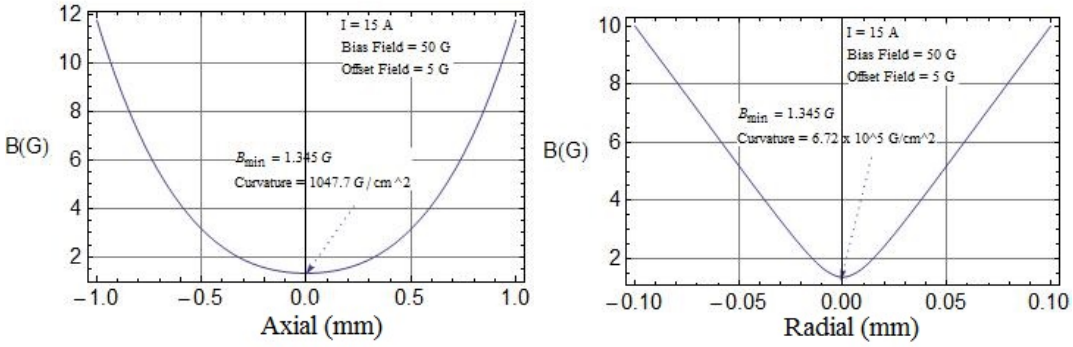

Figure 1.15: Variation of magnetic field along the axial and radial direction for a Ztrap. The axial and radial trap frequencies for the state F=2, m_F=2 in the ground state of Rb^{87} atom are calculated using the data derived from the above figure. The axial trap frequency is 41.24 Hz and similarly the radial trap frequency is 1044.65 Hz.

The current traveling through the wire affects these trap frequencies. As shown in the table 1.4.2, the axial and radial trap frequency varies as the current running through the wire increases.

Current in the Z-Wire(A)	Axial Trap Frequency(Hz)	Radial Trap Frequency(Hz)
10	34.054	1314.89
15	41.24	1044.65
20	50.177	813.551
25	53.294	708.044

Table 1.2: Variation of trap frequencies for an increasing value of current in the wire. At constant bias of 50 G and and B_{min} at the trap center adjusted to 1.5 G.

Effect of varying the dimensions of the wires:

Earlier in the case of a U-wire trap, we saw that increasing the thickness of the cross-wire leads to a change in the gradients of the quadrupole trap. In a similar manner, a change in the wire dimensions in a Z-wire reflects in the harmonic trap frequencies of the trap. In a Z-wire similar to the one discussed in this section, the width of the wire, its height and the current running through it are varied. It results in the following data:

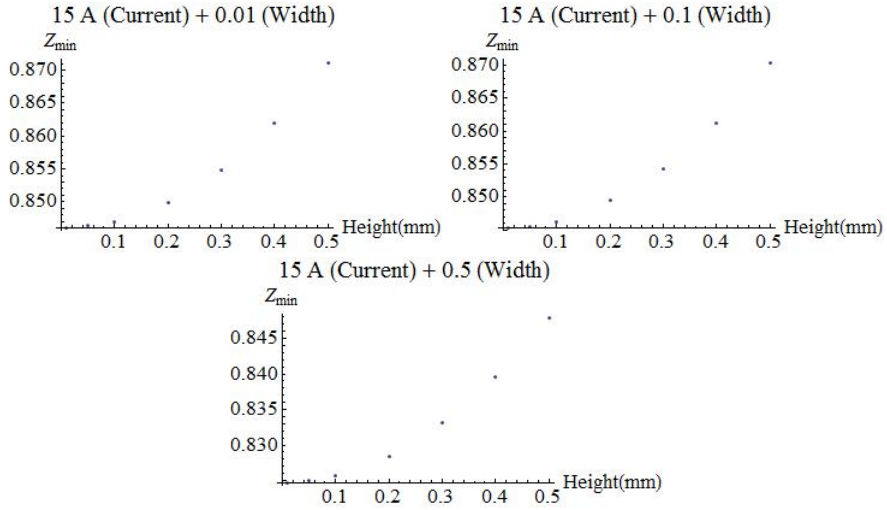

Figure 1.16: Variation of trap center distance with height of the wire for different widths and current in the wire.

Chapter 2

A magnetic micro-array of traps used as a Quantum Register

2.1 Array of Traps

A combination of Z and U-wire wires can be used create a series of potential wells. We call this series an array or a micro-array of traps. If we apply an external magnetic field $\mathbf{B} = \mathbf{20G}\ \hat{i} + \mathbf{10G}\ \hat{j}$ and send a current of 2A through the wire, each component interacts with the applied magnetic field and leads to the formation of following sequence of traps.

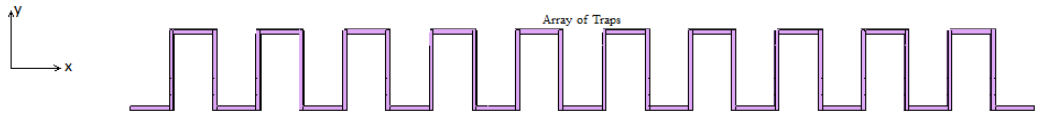

Figure 2.1: A combination of Z and U wires used to create an array of traps(array-wire). This array can be visualized as a series of Z-wires connected by horizontal sections of wires. The height of these sections as well as the cross-wire length is 200 μm and the length of the side-wires, 100μm.

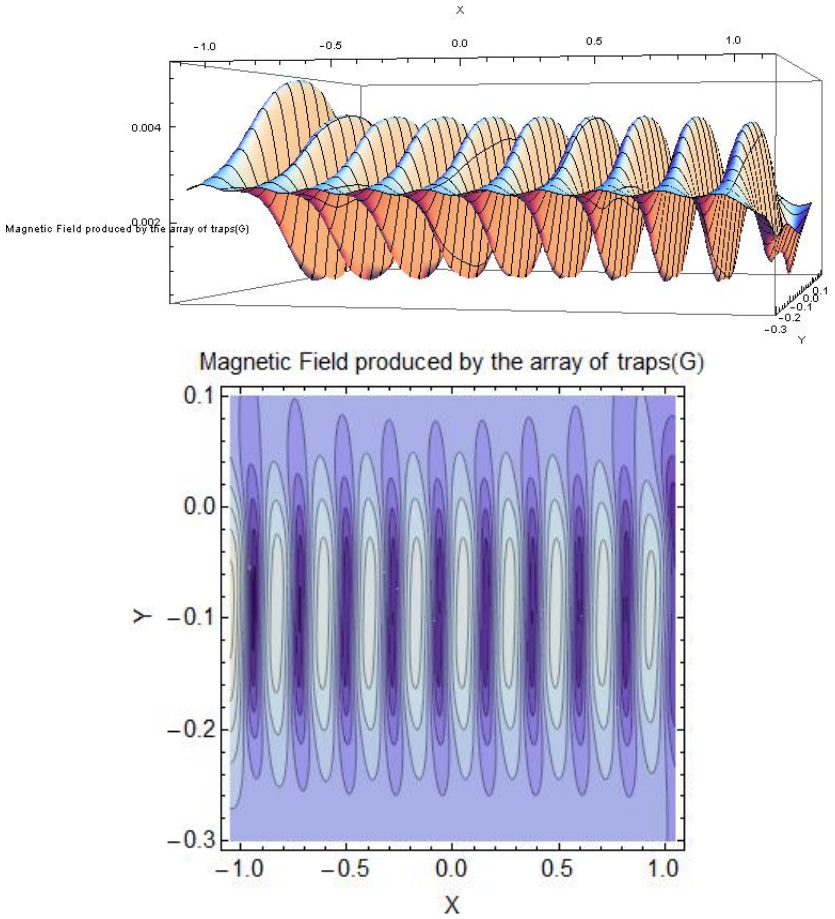

Figure 2.2: 3D-plot(left) and contour-plot(top) of magnetic field in the x-y plane and passing through the trap center on the Z-wire component which lies towards the middle of the array i.e. $Z = 78.16\mu m$.

In this array-of-traps picture, the trap centers for each of the Z wire components are not exactly at the same distance from the array-wire plane. It varies as one moves from one end of the array to the other. This can be seen in the figure 2.3. Furthermore, there is also a variation in the trap frequency across the length of the array.

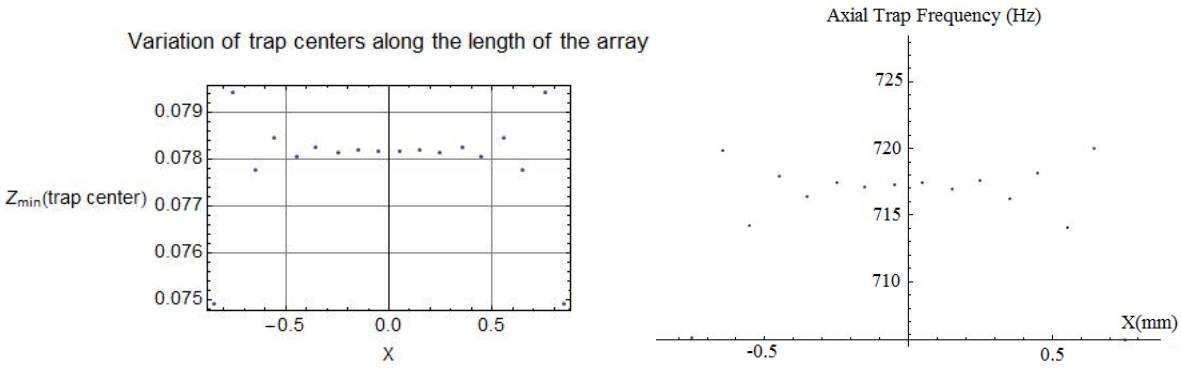

Figure 2.3: Variation of trap centers (on the left)and trap frequencies(right) across the length of the array.

Getting a knowledge of how the trap centers vary across this array is crucial in order to build a quantum register. Another theory which is important to know for creating a qubit register is of Rabi oscillations, which we will see in the next section.

2.2 Rabi Oscillations:

This section describes the semi-classical behavior of a quantum mechanical two-level system driven by a near resonant radiation. It briefly describes the oscillation of population of states which are known as Rabi Oscillations.

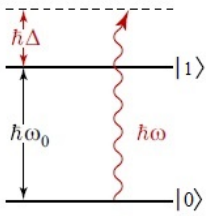

Figure 2.4: A two level system.

$|0\rangle$ and $|1\rangle$ are orthonormal basis for the system, $\langle i|j\rangle = \delta_{ij}$, $i, j = 0, 1$. The frequency of the photon is $\omega = \omega_o + \Delta$. Δ is the detuning between the frequency of the photon and resonant frequency ω_o.

In the absence of a driving electromagnetic field, the states $|0\rangle$ and $|1\rangle$ are the energy eigenstates of the system. Let $\hat{H}_o$ be the Hamiltonian of the system with no external applied field [9]. Therefore,

$$\hat{H}_o|0\rangle = 0|0\rangle \tag{2.1a}$$

$$\hat{H}_o|1\rangle = \hbar\omega_o|1\rangle \tag{2.1b}$$

A two level quantum state can be expressed as $|\psi\rangle = c_1|0\rangle + c_2|1\rangle$ where c_1 and c_2 are the amplitude for the states $|0\rangle$ and $|1\rangle$ respectively; and $|c_1|^2 + |c_2|^2 = 1$. The probability of finding the system in state $|i\rangle$ is $|\langle i|\psi\rangle|^2$=$|c_i|^2$, for i = 0,1.
An operator $\hat{A}$ can be represented by a 2× 2 hermitian matrix [9].

$$A = \begin{pmatrix} \langle 0|\hat{A}|0\rangle & \langle 0|\hat{A}|1\rangle \\ \langle 1|\hat{A}|0\rangle & \langle 1|\hat{A}|1\rangle \end{pmatrix} \tag{2.2}$$

The Hamiltonian $\hat{H}_o$ in case of no external electromagnetic field can be expressed as [9]

$$H_o = \hbar \begin{pmatrix} 0 & 0 \\ 0 & \omega_o \end{pmatrix} \tag{2.3}$$

However, if there is a driving field present, it induces a dipole moment between the states $|0\rangle$ and $|1\rangle$. The electromagnetic field interacts with this dipole and results in a perturbation. The interaction Hamiltonian can be represented as [9]

$$H_{int} = \hbar \begin{pmatrix} 0 & \Omega\cos(\omega t) \\ \Omega^*\cos(\omega t) & 0 \end{pmatrix}, \tag{2.4}$$

where $\hbar\Omega = \mu E_o$, μ is the induced dipole moment and E_o is the amplitude of the electromagnetic field. As a result of this perturbation, the states $|0\rangle$ and $|1\rangle$ are no longer stationary states of the system. Therefore, the two levels are said to be *coupled* due to the applied field.

2.2.1 Time Evolution of system under applied field: Rabi Oscillations

If the system starts from state $|0\rangle$ at $t = 0$,under the influence of an external applied field, the state amplitudes evolve as follows:

$$\begin{pmatrix} c_1(t) \\ c_2(t) \end{pmatrix} = \exp i\Delta t/2 \begin{pmatrix} \cos\frac{\Omega_R t}{2} + i\frac{\Delta}{\Omega_R}\sin\frac{\Omega_R t}{2} \\ i\frac{\Omega}{\Omega_R}\sin\frac{\Omega_R t}{2} \end{pmatrix}, \tag{2.5}$$

and therefore, the state probability amplitude evolve as

$$|c_2(t)|^2 = \frac{\Omega^2}{\Omega_R^2} \sin^2\left(\frac{\Omega_R t}{2}\right), \tag{2.6a}$$

$$|c_1(t)|^2 = \frac{\Delta^2}{\Omega_R^2} + \frac{\Omega^2}{\Omega_R^2} \cos^2\left(\frac{\Omega_R t}{2}\right). \tag{2.6b}$$

The above equations mean that the probability of the system being in state $|0\rangle$ and $|1\rangle$ oscillates with a frequency $\Omega_R = \sqrt{\Omega^2 + \Delta^2}$ (*total Rabi Frequency*). They also suggest that the states $|0\rangle$ and$|1\rangle$ are not the stationary states of the system anymore; which they indeed were in the absence of external applied field. Therefore, we can say that the dynamics of the system are governed by two parameters, the coupling strength which is proportional to E_o Ω and detuning Δ.

It is only on resonance when the populations oscillate completely between zero and unity. If there frequency of the photons and transition frequency are detuned, the oscillations are faster but of lower amplitude. Furthermore, for a fixed detuning, the frequency of the oscillations can be varied by changing the strength of the applied field.

Now that the evolution of the system beginning in state $|0\rangle$ is known, we consider the system to be at *resonance*($\Delta = 0$). Two specific cases are discussed:

- **A π pulse:** It corresponds to turning the field on at $t = 0$ and off at $t = T_\pi = \pi/\Omega$. From equation 2.5, we get:

  $$\psi(T_\pi) = \begin{pmatrix} 0 \\ i \end{pmatrix}, \tag{2.7}$$

  or, equivalently:

  $$|\psi(T_\pi)\rangle = i|1\rangle \tag{2.8}$$

  This state is equivalent to $|1\rangle$, and therefore, we can say that the *pi*-pulse transforms the state $|0\rangle$ into $|1\rangle$.

- **A $\pi/2$ pulse:** This corresponds to turning the field on at $t = 0$ and off at t= $T_{\pi/2}$= $\pi/2\Omega$. Consequently,

  $$\psi(T_{\pi/2}) = \frac{1}{\sqrt{2}} \begin{pmatrix} 1 \\ i \end{pmatrix}, \tag{2.9}$$

  or,

  $$|\psi(T_{\pi/2})\rangle = \frac{1}{\sqrt{2}}(|0\rangle + i|1\rangle). \tag{2.10}$$

This a superposition of the states $|0\rangle$ and $|1\rangle$. The probabilities of finding the system in each of the states is 1/2.

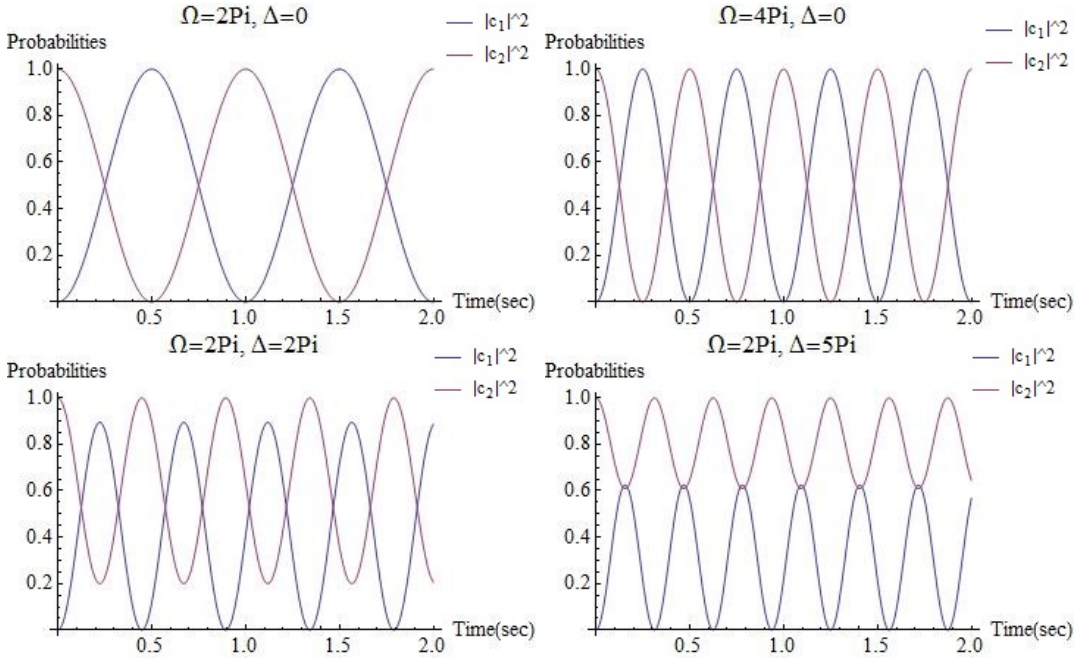

Figure 2.5: Plots for the oscillating probabilities of system in either state $|0\rangle$ or $|1\rangle$(red and blue lines respectively) for different sets if Rabi Frequencies and detuning.

2.3 Qubit Register

In section 1.1, we saw how the coupling between the total angular momentum **J** and the total nuclear angular momentum **I** is responsible for the Zeeman splitting of the fine-structure states. The $5^2S_{1/2}$ state further splits into the states F=1(m_F = -1,0,1) and F=2(m_F= -2,-1,0,1,2) Zeeman sublevels.

Let us consider two of these states i.e. $|F = 1, m_F = -1\rangle$ and $|F = 2, m_F = 1\rangle$ as $|0\rangle$ and $|1\rangle$ respectively. The array of traps described above can be used to trap atoms in one of the two states, i.e. $|0\rangle$ of $|1\rangle$ and create a quantum register. In order to achieve this, we first consider an array having 20 components (figure 2.6) and apply a bias-field of 30 G in the positive X direction.

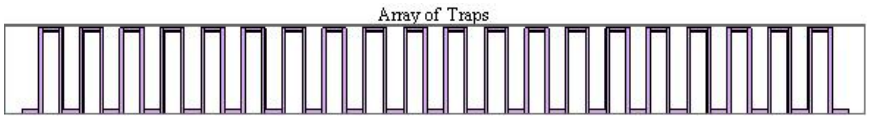

Figure 2.6: Top view of a one dimensional micro array (n=20) having individual component width = 5 μm, thickness of wire = 1μm, array height = 25 μm and conducting current I = 100 mA. This micro-array is used to create a quantum register.

If the micro-array is introduced in-between two parallel wires running perpendicular to the plane of the array, carrying a relatively higher current(6A) and far spaced from the array (900m away from the wire-array center), then there will be a field gradient of 50 G/mm created along the trap. This can be seen in the following figure:

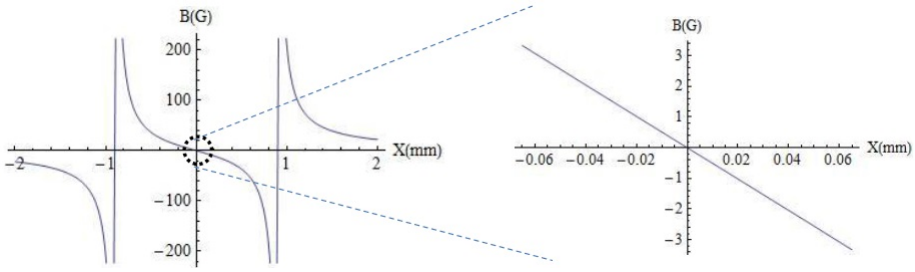

Figure 2.7: Gradient field created due to the additional wires running perpendicular to the plane of the array, carrying a relatively higher current(6A) and spaced 900m away from the wire-array center.

The aim of this exercise if to alter the magnetic field offset for each trap along the array (figure 2.8). This ensures that the energy gap between the two states $|0\rangle$ and $|1\rangle$ is different for different sites on the array. We would only want to expect a transition at the very specific site we choose, and a gradient field helps us achieve that goal. Each site corresponds to a different transition frequency.

Therefore, a transition at a particular chosen site can be achieved by interacting the atomic system with an electro-magnetic radiations of total frequency corresponding to the energy difference between the two states at that particular site.

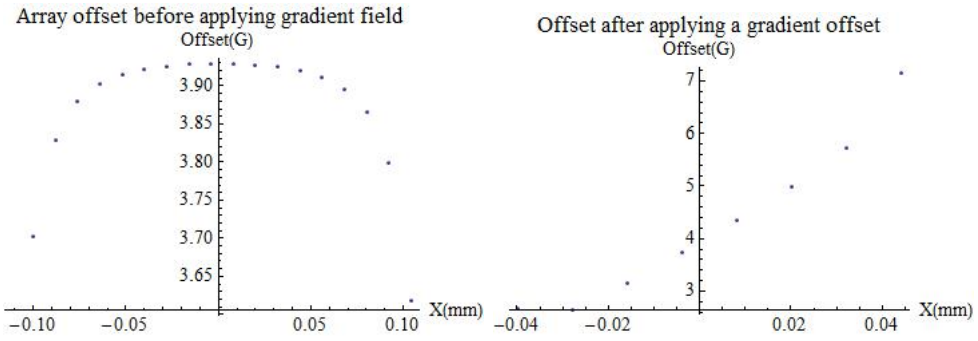

Figure 2.8: Trap offsets for each array site before and after the application of a gradient field.

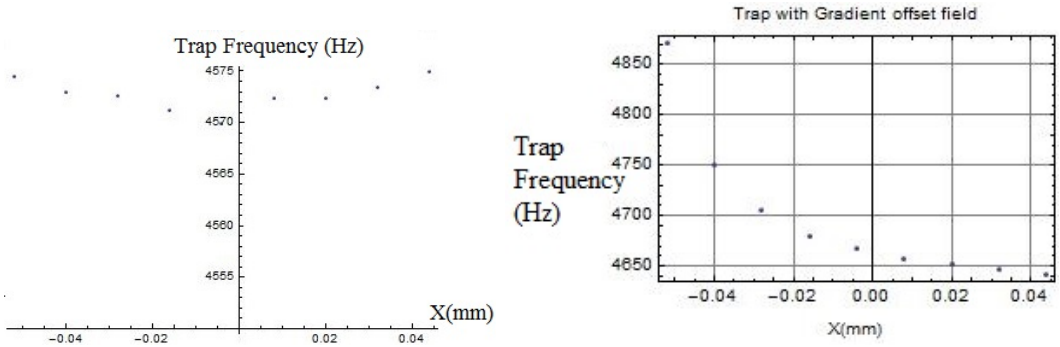

Figure 2.9: Trap frequency for each array site before and after the application of a gradient field(for ^{87}Rb; state: $F = 2$, $m_F = 2$).

The ground state levels $|0\rangle$ and $|1\rangle$ have the same first order Zeeman shift, and are separated by hyperfine splitting ($\omega_{hfs} \approx 6.8$ GHz). In the presence of an external magnetic field, the degeneracy in the hyperfine structure is broken and both levels (F = 1 and F = 2) experience a Zeeman splitting of $\pm$ 0.7 MHz/G between adjacent Zeeman levels. The $|0\rangle \leftrightarrow |1\rangle$ transition is a two photon excitation process as seen in the following figure.

The first photon is in the microwave range(≈ 6.8 Ghz) and the second is in the rf range (0.7 B_{off} MHz). The microwave frequency is detuned from $|1, -1\rangle \leftrightarrow |2, 0\rangle$ transition by Δ. δ represents the detuning of the total microwave and rf frequencies from the atomic transition frequency. As Δ is the detuning from the intermediate level, it is kept larger than each of the Rabi frequencies for individual microwave and rf transitions (Ω_{MW}^2 and $\Omega_{rf}^2 \ll \Delta^2$) such that probability for transition to the intermediate level is small.

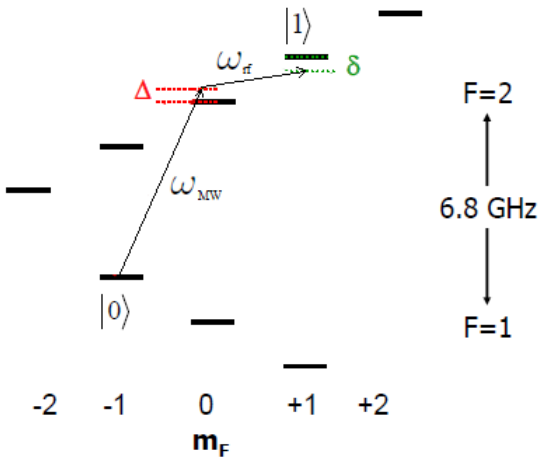

Figure 2.10: $^{87}Rb5S_{1/2}$ ground state with Zeeman splitting. The lines represent the microwave and rf radiation. $\Delta = \omega_{MW} - \omega_{|1,-1\rangle \leftrightarrow |2,0\rangle}$ and $\delta = \omega_{|0\rangle \leftrightarrow |1\rangle} - (\omega_{MW} + \omega_{rf})$.

The two photon transition Rabi frequency is given by [11]

$$\Omega_{Rabi} = \frac{\Omega_{MW}\Omega_{rf}}{2\Delta} \tag{2.11}$$

Therefore, we can creating getting a quantum register using a magnetic micro-array of neutral atom traps.

Chapter 3

Bose-Hubbard Model

Due to the Heisenberg uncertainty relation quantum fluctuations exist even at temperatures close to 0 Kelvin. These fluctuations can be strong enough to cause a phase transition from one phase to another. An example for this type of quantum phase transition is a change from a superfluid phase to a Mott insulator phase in a bosonic system where there is repulsive interaction between the particles and hopping through the lattice potential.

We consider an atomic gas of bosons at a low temperature such that a Bose-Einstein condensate is formed. When the condensate is subjected to a lattice potential in which the bosons can tunnel through from one site to the other, there are two states in which the system could be found:

- A ***superfluid*** phase, where the dominant kinetic energy is minimized by a delocalized wavefunction.
- A ***Mott insulator*** phase, which occurs when the repulsive atom-atom interactions are large as compared to the tunnelling(kinetic energy). The total energy is minimized when the occupancy of each site in the optical lattice is constant. The reduction in the atom number fluctuations lead to increased fluctuations in the phase.

  This phenomenon can be studied using the Bose-Hubbard model. In the Bose-Hubbard Hamiltonian, the kinetic energy and interaction energy terms compete against each other and this competition is fundamental to the quantum phase transition.

3.1 Bose-Hubbard Hamiltonian

The starting point of the Hamiltonian is the Gross-Pitaevskii equation [20]:

$$H = \int d^3r\psi^\dagger(r)\left[\frac{-\hbar^2\Delta^2}{2m} + V_o(r) + V_T(r)\right]\psi(r) + \frac{4\pi a_s\hbar^2}{2m}\int d^3r\ \psi^\dagger(r)\psi^\dagger(r)\psi(r)\psi(r) \tag{3.1}$$

where $\psi(r)$ is the boson field operator for atoms in a given internal atomic state, $V_o(r)$ is the optical lattice potential and $V_T(r)$ is a slow varying external trapping potential. The optical potential is of the form [19]:

$$V(x,y,z) = V_o(\sin^2(kx) + \sin^2(ky) + \sin^2(kz)) \tag{3.2}$$

with $k = 2\pi/\lambda$ being the wavevector, λ being the wavelength of the laser light which in turn corresponds to the lattice period $a = \lambda/2$; a_s is the s-wave scattering length and m is the mass of the atoms.

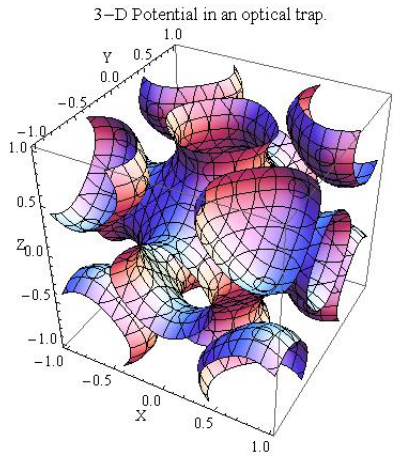

Figure 3.1: 3-D Contour Plot for the trapping potential $V(x,y,z)$

The energy eigenstates for the above hamiltonian are Bloch wave functions; and a superposition of these Bloch states yield a set of Wannier functions which are well localized on individual lattice sites. We can write the wavefunction in the wannier basis as $\psi(r) = \sum_i a_i w(r - r_i)$ [20]. The equation 3.1 reduces to[20]:

$$H = -J\sum_{<i,j>}\hat{a}_i^\dagger\hat{a}_j + \sum_i \epsilon_i\hat{n}_i + \frac{1}{2}U\sum_i \hat{n}_i(\hat{n}_i - 1) \tag{3.3}$$

where, $\hat{n}_i = \hat{a}_i^\dagger \hat{a}_i$ are the number operators which count the number of atoms at site i. $\hat{a}_i^\dagger$ and $\hat{a}_i$ are the creation and annihilation operators which follow the canonical commutation relations $\left[\hat{a}_i^\dagger, \hat{a}_j\right] = \delta_{ij}$.

$$J = -\int d^3 r w(r - r_i) \left(\frac{-\hbar^2 \Delta^2}{2m} + V_{lat}(r) \right) w(r - r_j) \tag{3.4}$$

is the hopping matrix element between two adjacent sites. It is the measure of tunneling between the sites of the lattice.

$$U = \frac{4\pi\hbar^2 a_s}{m} \int |w(x)|^4 d^3 x \tag{3.5}$$

is the on-site interaction matrix element. It is a measure of interaction energy between atoms at a particular site.

3.1.1 Superfluid Phase

When the tunneling term dominates in the Hamiltonian, the ground state energy is minimized if the single-particle wavefunctions of the atoms are spread over the entire lattice.

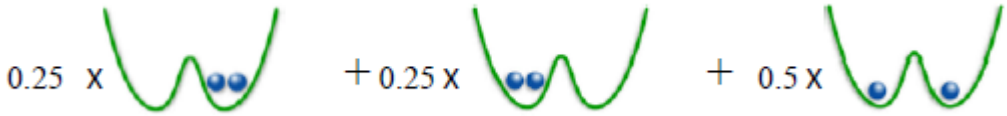

Figure 3.2: Superfluid state for two wells and two particles. The numbers 0.25 and 0.5 represent the probabilities of occurrence of a state

For 2 atoms and 2 lattice sites the wavefunction is:

$$\frac{1}{\sqrt{2}} (\phi_l + \phi_r) \otimes \frac{1}{\sqrt{2}} (\phi_l + \phi_r) \tag{3.6}$$

where ϕ_l and ϕ_r are the wave functions for the left and right side of the potential well respectively. Similarly, if there are M lattice sites and N atoms. The N-particle ground state is given by [19]

$$|\psi\rangle = \frac{1}{\sqrt{N}} \left(\frac{1}{\sqrt{M}} \sum_{i=1}^{M} \hat{a}_i^\dagger \right)^N |0\rangle \tag{3.7}$$

All atoms occupy the identical Bloch state. The probability distribution for the local occupation n_i of atoms on a single site is poisonian. The state is described by a macroscopic wavefunction with long range phase coherence throughout the lattice.

3.1.2 Mott Insulator state

If the interaction term dominates in the Hamiltonian, the system instead consist of localized wave-functions. There is a commensurate filling of atoms in the lattice sites, this essentially means that each site is occupied by a fixed number of atoms. The many body ground state is therefore a tensor product of local Fock states for each site.

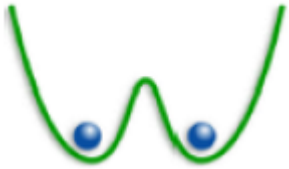

Figure 3.3: Mott insulator state for 2 wells and two particles

For 2 atoms and 2 lattice sites, the total wavefunction is:

$$\frac{1}{\sqrt{2}}\phi_l \otimes \phi_r + \frac{1}{\sqrt{2}}\phi_r \otimes \phi_l \tag{3.8}$$

Similarly for, M lattice sites and N atoms, the ground state of the many body system is given by [19]:

$$|\psi\rangle \propto \prod_{i=1}^{M} \left(\hat{a}_i^\dagger\right)^n |0\rangle, \tag{3.9}$$

where n is the number of atoms at per lattice site.

In this state phase coherence does not prevail in the system but there are perfect corelations in the atom number for the lattice sites.

When the strength of the interaction term relative to the tunnelling term is changed, the system reaches a quantum critical point for the ratio U/J. At this critical point, the system undergoes a quantum phase transition from a superfluid state to a Mott insulator state.

Chapter 4

Double Potential Wells

We consider two of the lattice sites discussed in section 3.1 as a double well problem and numerically study the variation of wavefunctions and tunnelling probability through the barrier, with increased lattice separation.
A double well potential can be defined as a quartic potential symmetric about the the y-axis:

$$V(x) = \frac{V_o}{b^4}(x^2 - b^2)^2 \tag{4.1}$$

where V_o is the potential at the local maxima which occurs at $x = 0$ and depends upon the mass of the atom(m) and oscillation frequency of the trap(ω). The next step is to solve the one dimensional time independent Schrodinger's equation for the above potential.

$$\left[\frac{-\hbar^2}{2m}\frac{d^2}{dx^2} + V(x)\right]|\psi\rangle = E|\psi\rangle. \tag{4.2}$$

where E is the eigen-energy for the Hamiltonian and ψ is the eigen-vector. The above potential can be solved analytically using WKB approximation [10]. But, I have numerically solved the equation 4.2.

4.1 Numeric solution for the quartic double well potential

The variables in our calculation are V_o and b. We compute the value of equation 4.2 with eigen-functions determined by a numerical solution to the Schrodinger's equation with the independent variable x in a defined range with parameter E(energy).

For the values $V_o = 2$ units, and b = 2 units, the wave functions overlap and renders a finite tunnelling probability (figure 4.1). The energy for the ground state wavefunction

is 0.90 units, while the energy for the first excited wave function is 0.94 units. These wavefunctions are not normalized yet.

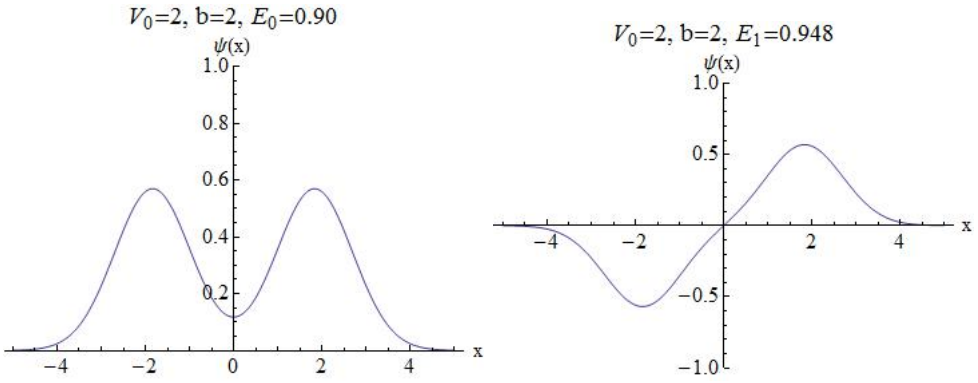

Figure 4.1: Ground state and first excited state wave functions for b = 2 units and V_o = 2 units.

Now, if we increase the separation between the two minima of the the potential function (equation 4.1) by increasing the value of b to 6 units, the overlap between the wavefunctions decreases as seen the following set of figures.

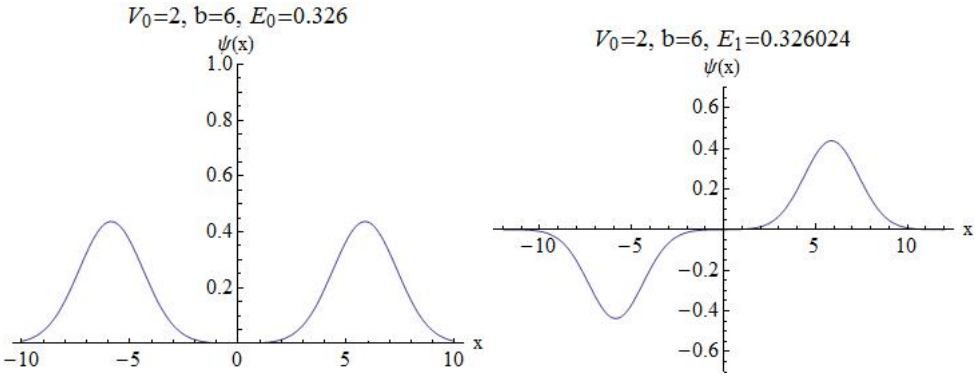

Figure 4.2: Ground state and first excited state wave functions for b = 6 units and V_o = 2 units

4.2 Tunnelling in a Double Well

The tunnelling probability T is calculated using the overlap integral of the two ground state wavefunctions for the individual well ψ_1 and ψ_2.

$$T \propto \int \psi_1 \psi_2 dx \tag{4.3}$$

But the question which arises here is how to find the individual ground state wave functions for each of the two sites. We know that the ground state wave function for a single harmonic well is gaussian.

$$\phi = \frac{1}{(\pi x_o)^{1/4}} \exp\left(-\frac{x^2}{2x_o}\right) \tag{4.4}$$

where $x_o = \hbar/m\omega$.

Therefore we can assume a gaussian wave function as the ground state for each site of the potential well.

$$f_1 = A \exp\left(-B(x-C)^2\right) \tag{4.5a}$$

$$f_2 = A \exp\left(-B(x+C)^2\right) \tag{4.5b}$$

Using the interpolation function values from the wavefunction calculated in section 4.1 we can find the value of the constants A, B and C, and hence the ground state wave functions ψ_1 and ψ_1 after normalizing f_1 and f_2 respectively.

As we can see from figure 4.2, the overlap between the wavefunctions decreases with increase in the value of b.

After recovering ψ_1 and ψ_2, we can calculate the overlap between the wave functions using equation 4.3 and therefore, the probability for an atom to tunnel across the potential barrier.

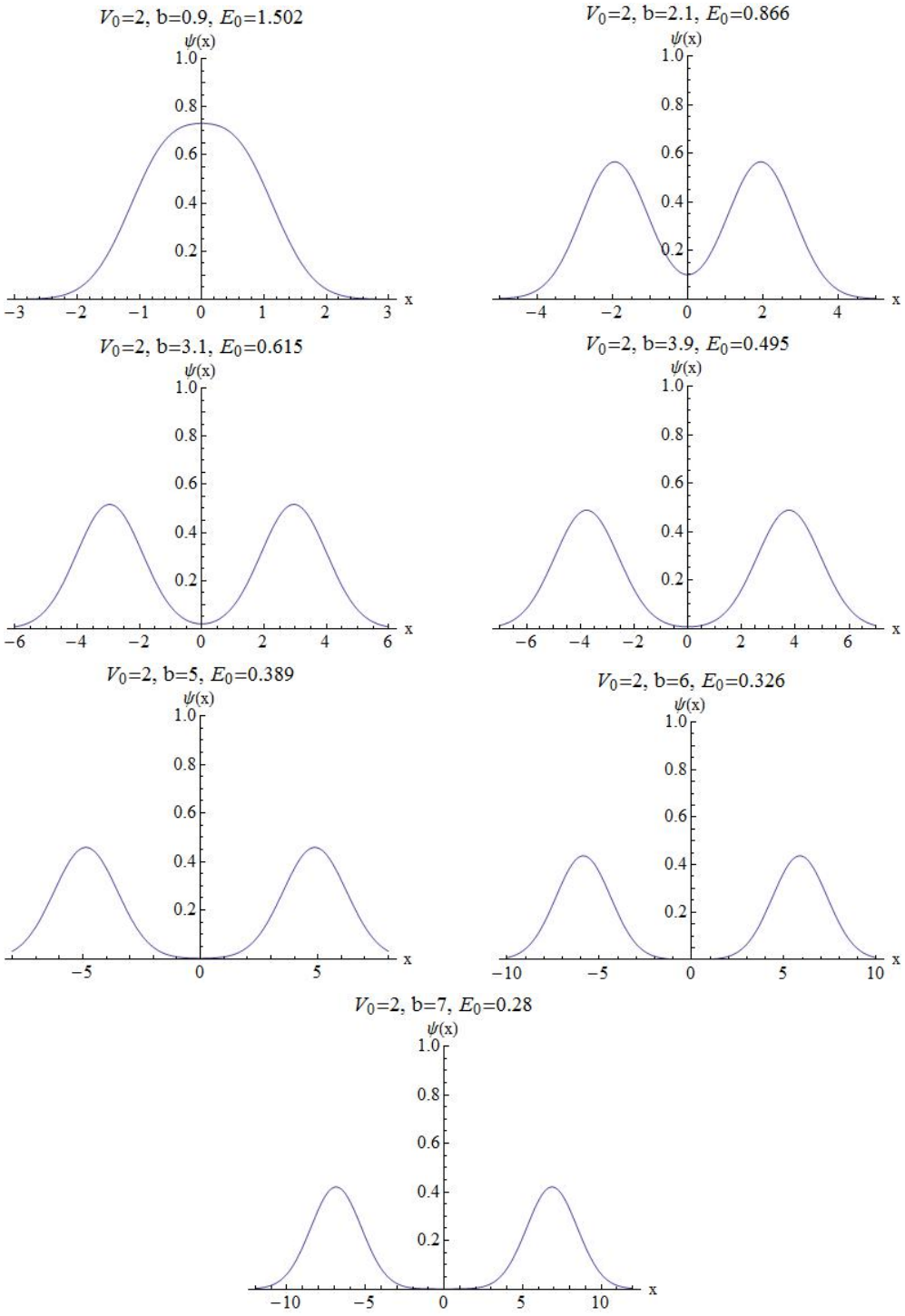

Figure 4.3: The wavefunctions for different values of b and at constant $V_o = 2$

The variation of the tunnelling probability can be easily observed from the plots or calculated. It varies with b as follows:

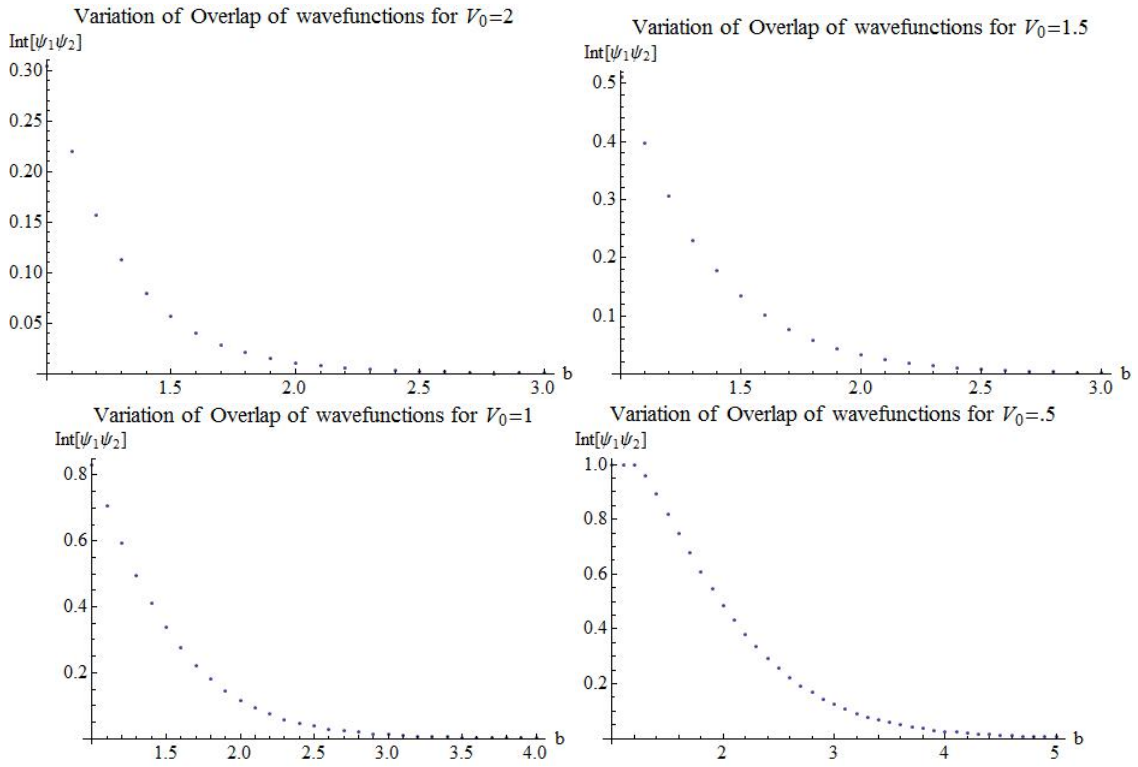

Figure 4.4: Variation of overlap of ground state wave functions for each site of the potential well(T). This is done for $V_o = 2$, $V_o = 1.5$, $V_o = 1$ and $V_o = 0.5$

As we can see in the above set of figures, the tunnelling probability alos varies with V_o. It increases as we increase V_0. However, for a particular value of V_o, we see an exponential decay of the tunnelling probability.

Chapter 5

Future Directions

We have seen in chapter 2 that a micro-array of magnetic traps for neutral atoms can be used to create a quantum register. The idea of a quantum register has been well explored by D. Schrader *et. al* [16], where they have used optical trapping potentials to trap atoms. Therefore, to produce a quantum register using magnetic traps for neutral atoms is a novel idea and can be pursued further. There is also an experimental scope for this project.

Bibliography

[1] *First Observation of Magnetically Trapped Neutral Atoms*, A.L. Migdall, J.V. Prodan, W.D. Phillips, T.H. Bergeman, H.J. Metcalf: Phys. Rev. Lett. **54**, 2596 (1985).

[2] Y. V. Gott, M. S. Ioffe, and V. G. Telkovskii, Nucl. Fusion Supplement **3**, 1045 (1962).

[3] *Cooling Neutral Atoms in a Magnetic Trap for Precision Spectroscopy*, D. Pritchard, Phys. Rev. Lett. **51**, 1336 (1983).

[4] *Continuous Stopping and Trapping of Neutral Atoms*, V. S. Bagnato, G. P. Lafyatis, A. G. Martin, E. L. Raab, R. N. Ahmad-Bitar, and D. E. Pritchard, Phys. Rev. Lett. **58**, 2194 (1987).

[5] *Microscopic Atom Optics: from wires to atom chip*, Ron Folman, Peter Kruger, Jorg Schmiedmayer, Johannes Denschlag, and Carstem Henkel, At. Mol. Opt. Physics **48**, 263-356 (2002).

[6] D. Cassettari, A. Chenet, J. Denschlag, R. Folman, B. Hessmo, A. Haase, P. Kruger, S. Schneider, and J. Schmiedmayer, in Laser Spectroscopy, XIV International Conference, edited by R. Blatt, J. Eschner, D. Leibfried, and F. Schmidt-Kaler (World Scientific,1999).

[7] *Atomic Micromanipulation with Magnetic Surface Traps*, J. Reichel, W. Hansel, and T. W. Hansch, Phys. Rev. Lett. **83**, 3398 (1999).

[8] *Trapping Atoms with a Wire*, A. Haase, D. Cassettari, B. Hessmo, and J. Schmiedmayer, Phys. Rev. A **64**, 043405 (2001).

[9] *Two-Level System : Rabi Oscillations*, Russell Anderson, 2008.

[10] *Double-Well Potential : The WKB Approximation with Phase Loss and Anharmonicity Eect*, Chang Soo Park, Myung Geun Jeong, Sahng-Kyoon Yoo, and D.K. Park, 1998.

[11] *The theory of coherent atomic excitations.* B.W. Shore, Wiley (1990).

[12] *Bose-Einstein Condensation(International Series of Monographs on Physics·*116*)*, Lev Pitaevskii and Sandro Stringari.

[13] *Microchip traps and Bose-Einstein Condensation*, J. Reichel, Appl. Phys. B 75, 469-487 (2002).

[14] *Rubidium 87 D Line Data,* Daniel A. Steck, available online at http://steck.us/alkalidata (revision 2.0.1,2 May 2008).

[15] *Design and construction of magnetic elements for trapping and transport of cold neutral atoms*, Marcius H. T. Extavour.

[16] *A neutral atom quantum register*, D. Schrader, I. Dotsenko, M. Khudaverdyan, Y. Miroshnychenko, A. Rauschenbeutel, and D. Meschede, Phy. Rev. Lett., **93**, 150501, 2004.

[17] W.H. Wing: Prog Quantum Electron. 8, 181 (1984).

[18] R. Frisch and E Serge, Z f. Physik 75, 610 (1933).

[19] *Quantum Phase Transition from a Superfluid to a Mott Insulator in a gas of ultracold atoms*, Marcus Greiner, Olaf Mandel, Tilman Esslinger, Theodor W. Hansch and Immanuel Bloch, Nature, **415**, (2002).

[20] *Cold bosonic atoms in optical lattices*, D. Jaksch, J.I. Cirac, C.W. Gardiner and P. Zoller, Phy. Rev. Lett., **81**, 3108-3111, 1998.

[21] Dr. Venkat Pai lecture notes, Cold Atoms Spring School, HRI, Allahabad.

[22] Wolfram Research, Inc., Mathematica, Version 9.0, Champaign, IL (2012).